JTTEE5 19:148–155
DOI: 10.1007/s11666-009-9356-8
1059-9630/$19.00 © ASM International

Failure of Thermal Barrier Coatings Subjected to CMAS Attack

L. Li, N. Hitchman, and J. Knapp

(Submitted April 21, 2009; in revised form June 9, 2009)

The effect of environmental deposits, such as calcium-magnesium-alumino-silicate (CMAS), on thermal barrier coatings (TBCs) of commercial grade was investigated in laboratory scale. A controlled CMAS infiltration was achieved through exposure of coatings to calibrated cement tape composites containing synthetic glass powder representative of CMAS. Tube furnace and cyclic thermal shock simulation equipment were utilized to melt the synthesized CMAS tape on coating surfaces. The resulting premature failures of coatings were investigated through study of the thermomechanical and thermochemical interactions between the coatings and CMAS deposit. It was found that the porous nature of the thermal-sprayed TBCs make them vulnerable to CMAS attack even before discernible chemical reaction starts. Possible mitigation approaches are proposed for a better coating life under such severe circumstances.

Keywords CMAS, environmental barrier, gas turbine, TBC, YSZ

1. Introduction

Airborne contaminants have been extensively investigated as a major cause of the early-life failure in jet engines which operate in dusty environments such as deserts or the vicinity of volcanic eruption plumes. The presence of these contaminant deposits is believed to trigger multiple adverse effects in gas turbine engines. In the cold and hot sections where temperatures are below the melting point of the contaminant particles, erosion of compressor components and blockage of cooling passages were reported by Smialek et al. (Ref 1) in their investigation of the loss of performance in Blackhawk helicopters operating in Persian Gulf. The contaminant particles were composed of mainly desert sand which was found to contain a calcium-aluminum silicate glass, low quartz, carbonates (dolomite and calcite), and some sodium chlorides (NaCl). Blockage of the flow paths and cooling holes in the hot section by the molten contaminant deposit was also found by Kim et al. (Ref 2) in their study of the disposition of volcanic materials in the hot sections of gas turbines. Although these investigations had not involved thermal barrier coatings (TBCs), their findings of deposition of glassy contaminants in engine components are relevant.

The 7 wt.% yittria-stabilized zirconia (7YSZ) TBCs currently in use rely on both the low thermal conductivity of the 7YSZ composition and the presence of porosity within the coating to provide a barrier to heat transport from the hot gas to the underlying bond-coated superalloy. The adverse effect of airborne contaminants on the early-life TBC degradation was also investigated in terms of erosive wear (at low temperatures) and thermomechanical and thermochemical attack (at high temperatures). Nicholls et al. (Ref 3) compared the erosion behavior of thermal spray and electron-beam physical vapor-deposited (EB-PVD) TBCs. Mercer et al. (Ref 4) proposed a coating delamination mechanism after molten CMAS infiltration, and Evans et al. (Ref 5) identified a number of material-removal mechanisms through observations of deformation and cracking of EB-PVD thermal barrier coatings. Toriz et al. (Ref 6) addressed that the deposition of gas stream molten debris would increase the coating stress due to the thermal expansion mismatch and cause spallation. In the study of degradation of TBCs in jet engine operating in Middle East route, Stott et al. (Ref 7) found that desert sand material consume free-standing TBC material aggressively during the test exposure at 1400 and 1500 °C.

Borom et al. (Ref 8) investigated the spallation of air-plasma-sprayed (APS) TBCs on power generation combustors, military turboshaft engines, and commercial turboprop engines. It was found that CaO, MgO, Al_2O_3, and SiO_2 (defined as CMAS, the acronym of each oxide), are incorporated in the molten phase that infiltrates the TBC microstructures. The differential thermal analysis of synthetic desert glass showed the melting of such kind of material is complete at 1290 °C.

This article is an invited paper selected from presentations at the 2009 International Thermal Spray Conference and has been expanded from the original presentation. It is simultaneously published in *Expanding Thermal Spray Performance to New Markets and Applications: Proceedings of the 2009 International Thermal Spray Conference*, Las Vegas, Nevada, USA, May 4-7, 2009, Basil R. Marple, Margaret M. Hyland, Yuk-Chiu Lau, Chang-Jiu Li, Rogerio S. Lima, and Ghislain Montavon, Ed., ASM International, Materials Park, OH, 2009.

L. Li, N. Hitchman, and **J. Knapp**, Praxair Surface Technologies, Inc., Indianapolis, IN. Contact e-mail: Li_Li@praxair.com.

Krämer et al. (Ref 9) systematically studied the thermochemical interaction of EB-PVD thermal barrier coatings with molten synthetic CMAS deposit. According to these authors, ''CMAS rapidly penetrates the open structure of the coating as soon as melting occurs, whereupon the original 7YSZ dissolves in the CMAS and reprecipitates with different morphology and composition that depends on the local melt chemistry''. Phase evolution during the interaction was also elucidated in their study in terms of available thermodynamic information.

In this article, the authors investigate CMAS attack on a number of TBCs of commercial grade with various typical coating microstructures. Experiments carried out in laboratory scale is yet to be prudently designed to be close to the real conditions encountered in the engines. Attack of molten CMAS on coatings is quantitatively compared. Mechanisms of coating failure caused by CMAS attack are scrutinized. The important role of coating microstructure at the incipience of CMAS attack is elucidated. A possible mitigation method is proposed in terms of delaying the molten CMAS infiltration and minimizing the penetration depth.

2. Experimental Details

2.1 CMAS Synthesis and Calibration

The CMAS powder was synthesized in Washington Mills Electro Minerals Co. (Niagara Falls, NY, USA). The nominal composition of the powder is listed in Table 1 which is close to what was reported elsewhere (Ref 8). In order to better control the amount of powder applied during the course of the experiment, it was ball milled to an average particle size of 27 μm. The particle size distribution is listed in Table 2. Systematic experiments of CMAS infiltration into coatings require a repeatable and reliable way to apply quantified CMAS powder for even infiltration into the coating system. A practice to achieve this goal originating from the University of California at Santa Barbara (Ref 10) is to fabricate tapes bounding various amounts of CMAS particles uniformly. The powder was weighted and then mixed with certain volume of cement 520 (Wall Colmonoy Corporation, Madison Heights, MI, USA). This particular cement was selected because it burns out leaving no residual above 550 °C. After evaporation of the solvent, the mixture consists of thick slurry that can be cast into a flat Teflon mold with a dimension of 140 mm × 89 mm × 0.13 mm. After drying, a thin sheet of cement-bonded CMAS particles was formed that could be readily cut to the desired shape and size and positioned on top of coatings of interest. In order to calibrate the CMAS concentration in the cement sheet, samples from four corners of the sheet were cut to 1-cm diameter and burnt in the furnace up to 600 °C. The powder residual was then weighed to determine the concentration in grams of CMAS powder per square centimeter. Table 3 lists several CMAS cement sheet made in this study.

Table 1 Nominal composition of the synthesized CMAS powder

Oxides:	CaO	MgO	Al_2O_3	SiO_2	Fe_2O_3	Other
wt.%	32.90	7.23	12.68	46.71	0.41	Balance

Table 2 CMAS powder particle size distribution

Volume, %:	3	10	50	90	94
Size, μm	>75.02	>64.67	29.68	>10.36	>8.47

2.2 Infiltration Process and Characterization

The YSZ thermal barrier coating system of commercial grade and some experimental coating systems provided by Praxair Surface Technologies Inc. (Indianapolis, IN, USA) were subjected to CMAS attack in this study, as listed in Table 4. The coating porosities were determined through Archimedes' Principle (ASTM B328-96) on free standing coatings prepared at the same spray conditions as those for CMAS infiltration, which were applied on HASTELLOY-X buttons with a diameter of 25.4 mm and a thickness 3.2 mm. CMAS tapes of 25.4 mm diameter with one of the concentrations listed in Table 3 were glued on to top of the coating surfaces using the cement 520. The infiltration process was accomplished either in a tube furnace or through a flame burner. The CMAS infiltration through a tube furnace was implemented by sliding samples topped with a CMAS tape in a furnace tube preheated to 1000 °C. The furnace temperature was then raised to 1300 °C in 30 min and maintained for additional 90 min before being cooled down to 1000 °C (within 30 min). Subsequently, samples were removed from the furnace and air cooled to room temperature. For the flame burner, an oxygen-propylene flame was utilized to melt and infiltrate the CMAS into the different coatings. The burner was set up so that the flame was in the horizontal position and the sample surface was perpendicular to it. Table 5 summarizes the typical burner set up for infiltration purposes. The front and back surface temperatures

Table 3 CMAS cement tapes

CMAS concentration level	Concentration, g/cm^2
Low	3
Medium	13, 14
High	22, 23

Table 4 TBCs subjected to CMAS attack

Coating name	Deposition method	Materials	Thickness, μm	Porosity, %
Low density	Air plasma spray	7YSZ	610	15
Dense vertically cracked (DVC)	Shroud plasma spray	7YSZ	762	8
D-gun YSZ	Detonation spray	7YSZ	406	6

were measured with a two-color pyrometer at wavelengths of 0.75 and 1.05 μm, respectively. CMAS-attacked samples were characterized meticulously through scanning electron microscopy to elucidate the physical interaction of molten CMAS on various coating structures. Possible chemical reactions were examined through x-ray diffraction (XRD) using the Cu Kα illumination.

3. Results

3.1 Macro/Microstructure Evaluation

3.1.1 Typical Failure Mode. A mud-flat cracked texture and coating delamination has been previously reported in a Far East combustor venturi (Ref 8). A similar failure mode is observed in dense vertically cracked (DVC) YSZ samples subjected to a 90-s burner infiltration followed by a 2000-cycle test. A typical test cycle consists of a 20-s heating, a 20-s forced nitrogen cooling, and a 40-s dwelling in ambient air (Ref 11). The layered spallation mode of the dense vertically cracked YSZ coating after the CMAS attack is observed on the surface (Fig. 1a and b). Please note that after 2000-cycle test, most of the CMAS-infiltrated YSZ has spalled off. A cross-sectional view (Fig. 1c) reveals that the spallation cracks, underneath the CMAS-contaminated area, run through the YSZ coating parallel to the interface. On the other hand, for the tube furnace-infiltrated DVC sample, a glassy matrix is observed in the CMAS-accumulated area with dissolved YSZ particles present within. The porous coating structure is replaced by a densified composite (as shown in Fig. 1d). Frothing, once reported by Borom et al. (Ref 8), is also evidenced during the dissolving process (Fig. 1d).

Table 5 Flame burner set up

Oxygen, slm	Propylene, slm	Standoff distance, mm	Heating time, s
7.53	3.70	127	60-200

3.1.2 Effect of the Area Density of the CMAS Powder. The CMAS infiltration with tapes having two different powder concentrations (14 and 22 g/cm^2) were compared to elucidate the possible relationship between the amounts of infiltrated CMAS powder and the resulting penetration depth in the ceramic coating. It is surprising to observe that the CMAS infiltration had almost an identical penetration depth (150-250 μm) in both cases (Fig. 2). The residual glassy material is accumulated on top of the coating surface. A thicker residual CMAS layer was observed in the case of 22 mg/cm^2 infiltration compared to that of 14 mg/cm^2 infiltration. Unless delamination occurs, the dense layer formed after the infiltration works as a barrier to prevent further CMAS attack into the inner coating structure.

3.1.3 Effect of the Coating Structure. The resistance to CMAS attack of various coating structures was

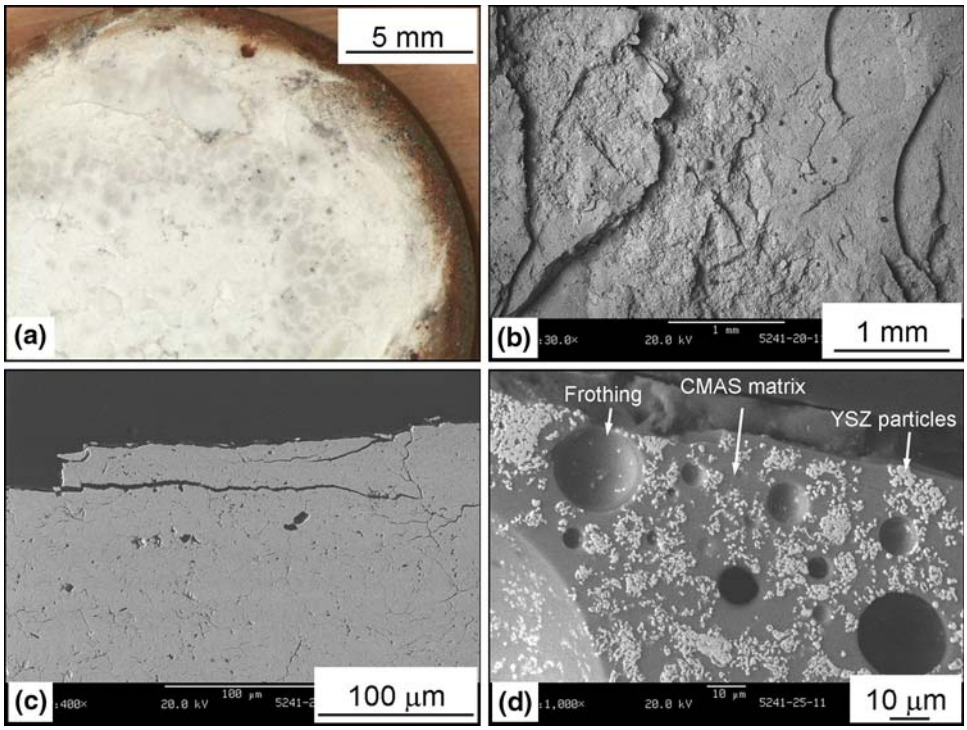

Fig. 1 Surface (a, b) and cross-sectional (c, d) views of the CMAS-attacked dense vertically cracked YSZ coating. (a-c: 90-s burner infiltration followed by 2000-cycle test, The CMAS tape used had an area density of 14 g/cm^2; d: furnace infiltration with a CMAS tape of area density of 22 g/cm^2)

investigated. Low density (~15% porosity), dense vertically cracked YSZ (~8% porosity), and D-gun YSZ (~6% porosity) coatings were infiltrated with the CMAS powder at an area density of 13 g/cm^2. It is found that after the infiltration, the low density coating (Fig. 3a) is completely soaked with CMAS and is crumbled into multiple layers with ~0.5 mm for each layer; DVC (Fig. 3b) and D-gun YSZs (Fig. 3c) hold their structural integrity fairly well, and the surface contamination is more prevalent for the DVC sample. The D-gun YSZ coating seems intact—only large drops of CMAS residue is left on its surface.

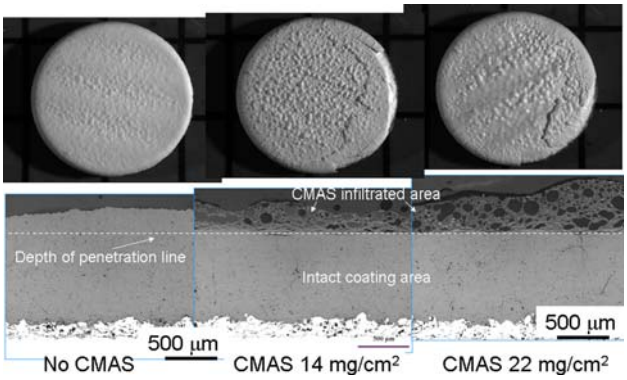

Fig. 2 Surface (top) and cross-sectional (bottom) views of the dense vertically cracked YSZ coatings infiltrated by the CMAS powder with two different area densities (furnace infiltration). The diameters of the buttons are approximately 25.4 mm

3.2 Study of Incipience of CMAS Attack

As denser coatings demonstrate a higher potential to resist the CMAS attack (as shown in Fig. 3), it would be interesting to quantify the resistance in terms of time and study the dynamics of the CMAS attack on such dense coating structures. The DVC YSZ (~8% porosity) and D-gun YSZ (~6% porosity) were chosen for the CMAS infiltration (area density 13 g/cm^2) using the oxy-fuel flame setup until a noticeable reaction occurred.

3.2.1 CMAS Attack on the DVC Coating. The DVC YSZ coatings topped with the CMAS tapes were heated by the flame for 60 and 90 s, respectively. After 60 s of heating, there is less sign of a reaction (Fig. 4a). The CMAS powder is molten and accumulated on top of the coating surface. It is worth noting that the 60-s infiltration image shown in Fig. 4(a) looks different from what is shown in Fig. 3(b). The reason is that the CMAS glassy shell delaminated during the handling of the sample shown in Fig. 3(b). Noticeable attack of the CMAS occurred after 90-s heating of the flame as shown in Fig. 4(b). This attack was denoted by the frothing phenomenon (as shown in Fig. 5a and b). Molten CMAS finds its way into the cracked area and solidify inside the coating when temperature is below its melting point. The solidified CMAS that is captured in the middle of a vertical crack is shown in Fig. 5(c) and (d).

3.2.2 CMAS Attack on the D-gun YSZ Coating. The similar infiltration test was also performed on the D-gun YSZ. Figure 6 illustrates the dynamics of the CMAS attack on the D-gun YSZ after 60-s (Fig. 6a), 90-s (Fig. 6b),

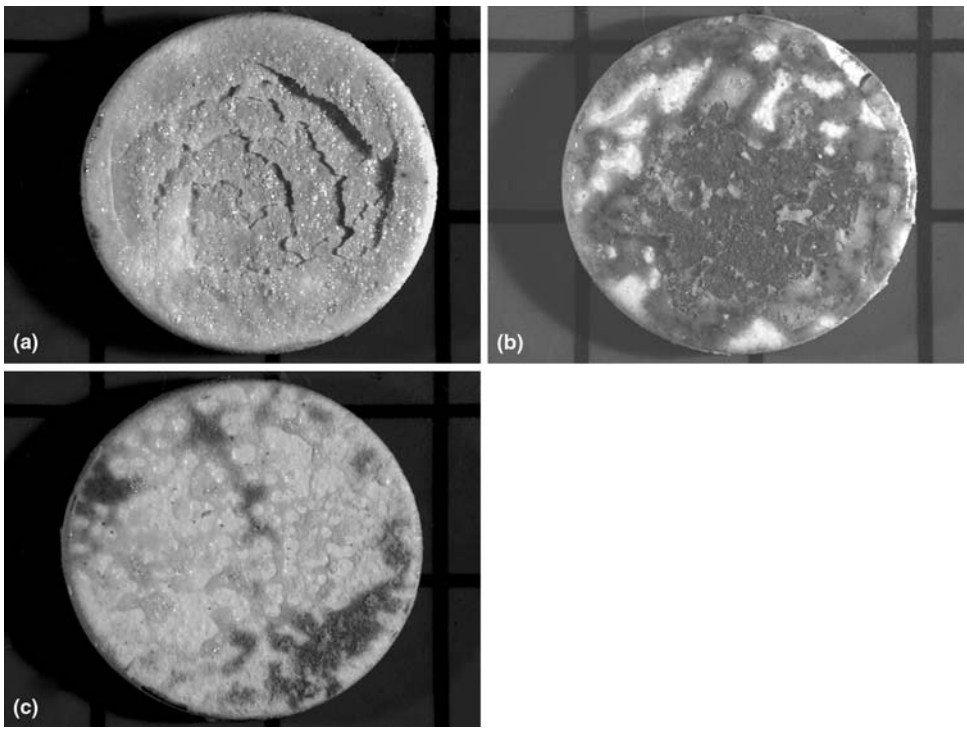

Fig. 3 Surface views of (a) low density, (b) DVC YSZ, and (c) D-gun YSZ coatings infiltrated by the CMAS powder with the same area density, 13 g/cm^2 (60-s burner infiltration). The diameters of the buttons are approximately 25.4 mm

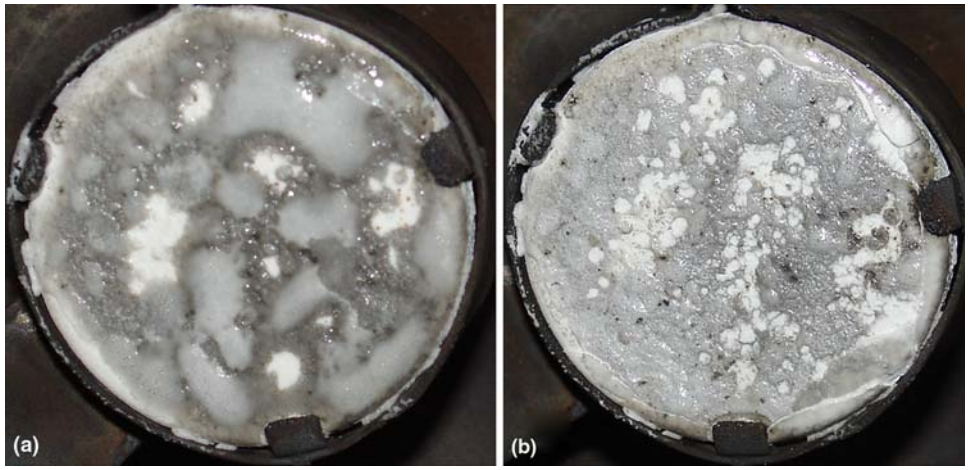

Fig. 4 Dynamics of the CMAS attack on the DVC structures after (a) 60-s and (b) 90-s heating with the oxy-fuel flame. The CMAS tape used had an area density of 13 g/cm^2. The diameters of the buttons are approximately 25.4 mm

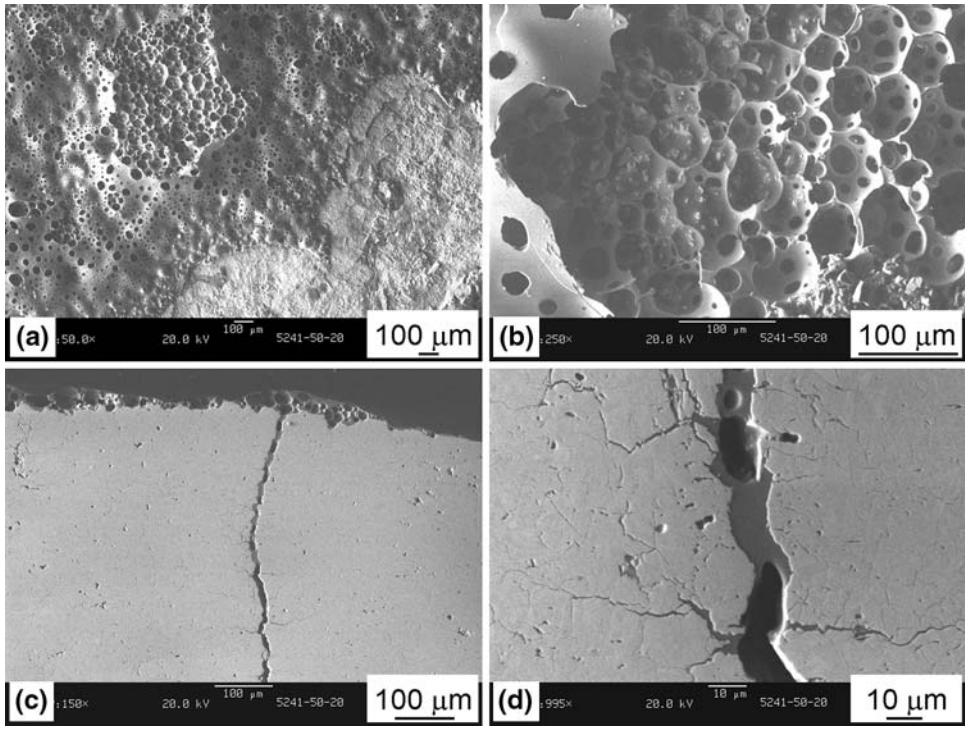

Fig. 5 Surface (a, b) and cross-sectional (c, d) views of the CMAS attack of the DVC YSZ, after 90-s heating with oxy-fuel flame. The CMAS tape used had an area density of 13 g/cm^2

and 150-s (Fig. 6c) heating of the oxy-fuel flame. It seems that the remarkable reaction occurred in about 150 s. However, even after 150 s, the contaminated areas still have a fairly uniform coating surface structure. Bubbles were observed on the surface of contaminated area (Fig. 7a and b). Cross-sectional views (Fig. 7c and d) reveal a pool of glassy material flowing on top of the coating surface with fewer bubbles compared to that in Fig. 5.

3.3 XRD of the Infiltrated and the Non-infiltrated YSZ

Possible chemical reactions of YSZ coatings with CMAS were examined by means of XRD. Krämer et al. (Ref 9) found that during the chemical reaction, CMAS causes a significant yttrium depletion out of the YSZ system, which leads to a monoclinic phase transformation of the YSZ coating. Tube furnace infiltrated and

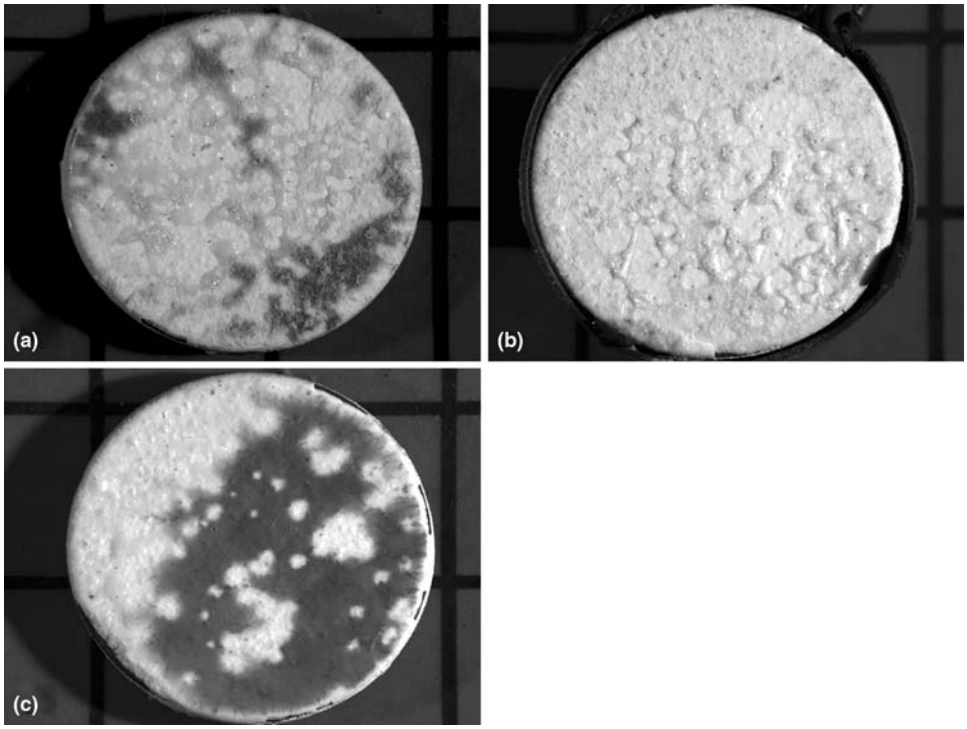

Fig. 6 Dynamics of the CMAS attack on the D-gun YSZ after (a) 60-s, (b) 90-s and (c) 150-s heating with the oxy-fuel flame. The CMAS tape used had an area density of 13 g/cm^2. The diameters of the buttons are approximately 25.4 mm

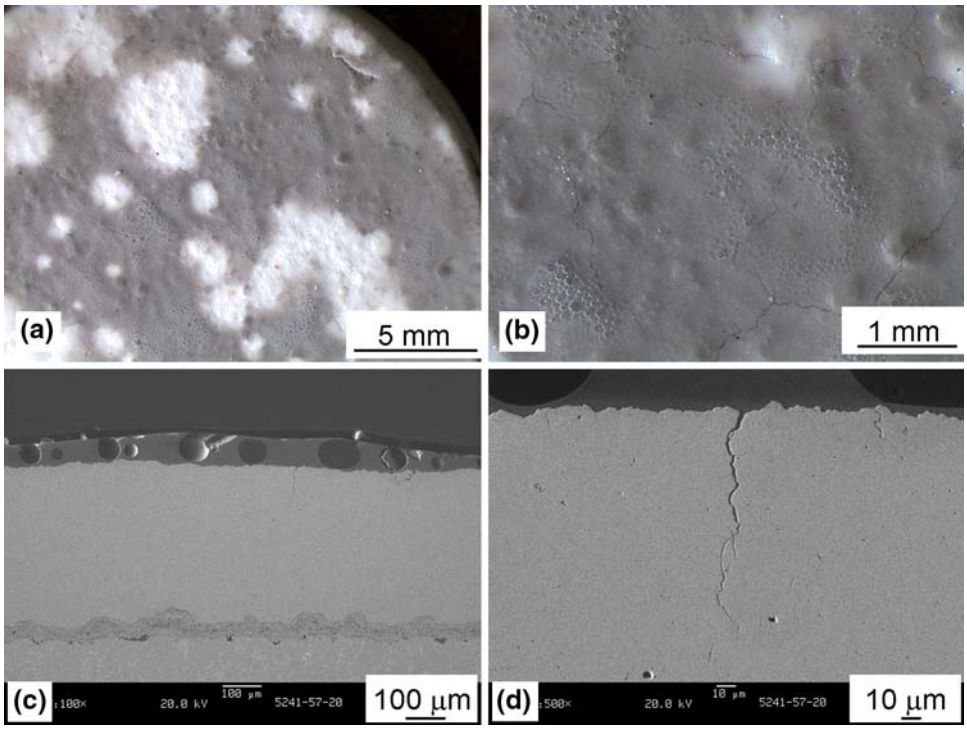

Fig. 7 Surface (a, b) and cross-sectional (c, d) views of the CMAS attack of the D-gun YSZ, after 150-s heating with oxy-fuel flame. The CMAS tape used had an area density of 13 g/cm^2

burner-infiltrated DVC YSZ samples were characterized using XRD. Only samples infiltrated with CMAS in the tube furnace showed noticeable monoclinic peaks (Fig. 8a). In order to eliminate the possible process effect of heat treatment *per se*, a non-infiltrated coating was put into the furnace and subjected to the same heat treatment

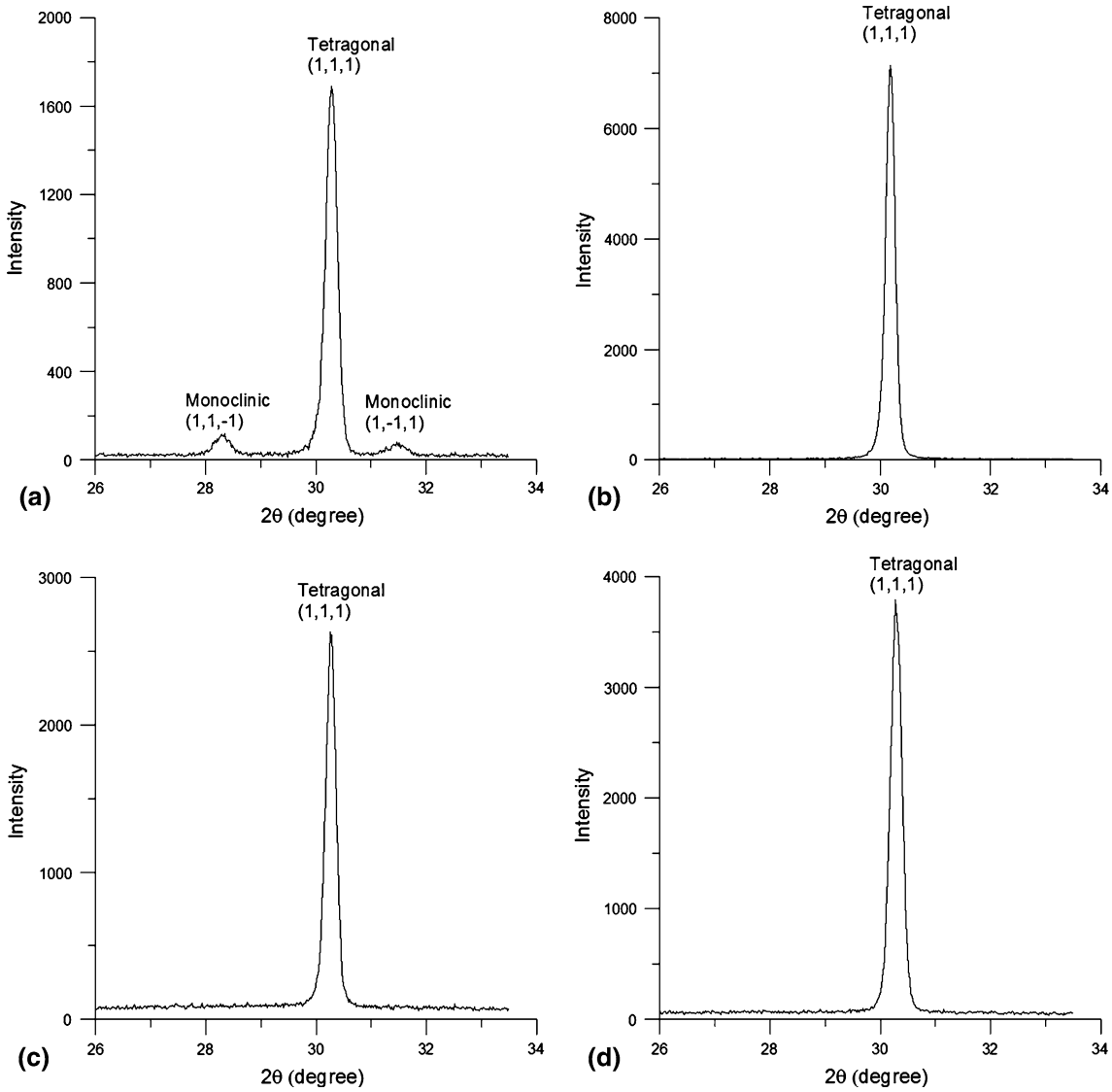

Fig. 8 XRD results of multiple dense YSZ coatings with or without CMAS attack: (a) 2-h furnace infiltration; (b) 2-h furnace heat treatment without CMAS infiltration; (c) 60-s oxy-fuel burner infiltration; (d) 90-s oxy-fuel burner infiltration. The CMAS tape used had an area density of 13 g/cm^2

process together with the infiltrated sample. No monoclinic peaks are detected on the non-infiltrated coating (Fig. 8b), which suggests that the monoclinic phase transformation is induced by the chemical attack of CMAS. However, this kind of attack is not observed in the burner-infiltrated YSZ coatings (Fig. 8c and d) due to very limited interaction time, i.e., 60-90 s compared to 2 h for furnace infiltration.

4. Discussion

The CMAS attack on thermally sprayed YSZ coatings is very aggressive due to the coating splat-layered structure. The CMAS dissolving process densifies the affected area by attacking the micro cracks and splat boundaries first. However, frothing of the reaction generates new kind of porosities. The cause of the frothing phenomenon is still under debate. One possible reason is that the air within the porous coating structure tries to escape from it and is trapped within the solidified CMAS layer, which can be seen in Fig. 5 and 7. A further infiltration of CMAS may be retarded by the original, reacted layer. The coating failure observed in this study involves the spallation of the top layer coating which has been infiltrated with the CMAS. The incipience of the CMAS attack seems to involve only the physical damages. The discernible chemical attack requires a long term interaction between the molten CMAS and YSZ

materials. In this study, only the infiltration in the tube furnace (2 h) resulted in a detectable chemical reaction. Because of the porous nature of thermally sprayed coatings, the CMAS attack can lead to a catastrophic coating failure in a relatively short time period—even before a noticeable chemical reaction sets forth. It is also found in this study that the coating density has an impact on the dynamics of the CMAS attack. A denser coating has a potential to resist the CMAS attack for a longer time than a more porous coating. Based on this finding, a dense cap layer may be envisioned as a potential mitigation technique.

5. Summary

An experimental methodology to approach the problem of CMAS attack on TBCs has been investigated. The coating degradation simulated in this method is similar to reports from field studies of aircraft engines. This methodology may assist in the evaluation of mitigating solutions for CMAS attack. Mitigation concepts under investigation include high-density cap layers.

Acknowledgments

The authors would like to thank Don Charles and James Parr for their help in sample preparation, Dr. Anthony Starvros and Brian Thompson for their help in furnace and burner operations, Gregory Moody and Randy Mock for their help in metallographic sample preparations, Carl Rice Jr., for his help in SEM, Marina Berezhev for her help in XRD, and Dr. Albert Feuerstein for his valuable discussions. The authors especially thank Dr. Thomas Taylor for his kind assistance.

References

1. J.L. Smialek, F.A. Archer, and R.G. Garlick, The Chemistry of Saudi Arabian Sand: A Deposition Problem on Helicopter Turbine Airfoils, *Advances in Synthesis and Processes, 3rd Int. SAMPE Metals Conf.* F.H. Froes, et al., Ed., October 20-22, 1992, p M63-M77
2. J. Kim, M.G. Dunn, A.J. Baran, D.P. Wade, and E.L. Tremba, Deposition of Volcanic Materials in the Hot Sections of Two Gas Turbine Engines, *ASME Trans. J. Eng. Gas Turbines Power*, 1993, **115**(3), p 641-651
3. J.R. Nicholls, M.J. Deakin, and D.S. Rickerby, A Comparison Between the Erosion Behaviour of Thermal Spray and Electron Beam Physical Vapour Deposition Thermal Barrier Coatings, *Wear*, 1999, **233-235**, p 352-361
4. C. Mercer, S. Faulhaber, A.G. Evans, and R. Darolia, A Delamination Mechanism for Thermal Barrier Coatings Subject to Calcium-Magnesium-Alumino-Silicate (CMAS) Infiltration, *Acta Mater.*, 2005, **53**(4), p 1029-1039
5. A.G. Evans, N.A. Fleck, S. Faulhaber, N. Vermaak, M. Maloney, and R. Darolia, Scaling Laws Governing the Erosion and Impact Resistance of Thermal Barrier Coatings, *Wear*, 2006, **260**(7-8), p 886-894
6. F.C. Toriz, A.B. Thakker, and S.K. Gupta, Thermal Barrier Coatings for Jet Engines, *J. ASME*, 88-GT-279, 1988 (presented at the Gas Turbine and Aeroengine Congress Amsterdam, The Netherlands, June 6-9, 1988)
7. F.H. Stott, D.J. de Wet, and R. Taylor, The Effect of Molten Silicate Deposits on the Stability of Thermal Barrier Coatings for Turbine Applications at Very High Temperatures, *Advances in Synthesis and Processes, SAMPE*, F.H. Froes, et al., Ed., 1992, Vol. 3, p M92-M101
8. M.P. Borom, C.A. Johnson, and L.A. Peluso, Role of Environmental Deposits and Operating Surface Temperature in Spallation of Air Plasma Sprayed Thermal Barrier Coatings, *Surf. Coat. Technol.*, 1996, **86-87**(1), p 116-126
9. S. Krämer, J. Yang, C.G. Levi, and C.A. Johnson, Thermochemical Interaction of Thermal Barrier Coatings with Molten CaO-MgO-Al_2O_3-SiO_2 (CMAS) Deposits, *J. Am. Ceram. Soc.*, 2006, **89**(10), p 3167-3175
10. L. Li and D.R. Clarke, Effect of CMAS Infiltration on Radiative Transport Through an EB-PVD Thermal Barrier Coating, *Int. J. Appl. Ceram. Technol.*, 2008, **5**(3), p 278-288
11. A. Bolcavage, A. Feuerstein, J. Foster, and P. Moore, Thermal Shock Testing of Thermal Barrier Coating/Bondcoat Systems, *J. Mater. Eng. Perform.*, 2004, **13**(4), p 389-397